European Journal of Neurology

european journal of neurology
the official journal of the european academy of neurology

ORIGINAL ARTICLE OPEN ACCESS

An Investigation of Corticospinal Tract Microstructural Integrity in ARSACS Using a Profilometry MRI Analysis: Results From the PROSPAX Study

Alessandra Scaravilli[1] | Gaia Mari[2] | Ilaria Gabusi[2] | Matteo Battocchio[2] | Sara Bosticardo[2] | Simona Schiavi[2] | Benjamin Bender[3] | Christoph Kessler[4] | Roberta La Piana[5,6] | Bart P. van de Warrenburg[7] | Mirco Cosottini[8] | Dagmar Timmann[9] | PROSPAX Consortium | Alessandro Daducci[2] | Rebecca Schüle[4,10,11] | Matthis Synofzik[10,12] | Filippo Maria Santorelli[13] | Sirio Cocozza[1]

[1]Department of Advanced Biomedical Sciences, University of Naples "Federico II", Naples, Italy | [2]Department of Computer Science, Diffusion Imaging and Connectivity Estimation (DICE) lab, University of Verona, Verona, Italy | [3]Department of Diagnostic and Interventional Neuroradiology, University of Tübingen, Germany | [4]Center for Neurology and Hertie Institute for Clinical Brain Research, University of Tübingen, Tübingen, Germany | [5]Department of Neurology & Neurosurgery, Montreal Neurological Institute, McGill University, Montreal, Canada | [6]Department of Diagnostic Radiology, McGill University, Montreal, Canada | [7]Department of Neurology, Donders Institute for Brain, Cognition, and Behaviour, Radboud University Medical Center, Nijmegen, the Netherlands | [8]Department of Translational Research on New Technologies in Medicine and Surgery, University of Pisa, Pisa, Italy | [9]Department of Neurology and Center for Translational Neuro- and Behavioral Sciences (C-TNBS), Essen University Hospital, Essen, Germany | [10]German Center for Neurodegenerative Diseases (DZNE), Tübingen, Germany | [11]Division of Neurodegenerative Diseases, Department of Neurology, Heidelberg University Hospital and Faculty of Medicine, Heidelberg, Germany | [12]Division Translational Genomics of Neurodegenerative Diseases, Center for Neurology and Hertie Institute for Clinical Brain Research, University of Tübingen, Tübingen, Germany | [13]Department of Molecular Medicine, IRCCS Stella Maris Foundation, Pisa, Italy

Correspondence: Filippo Maria Santorelli (filippo3364@gmail.com)

Received: 9 May 2024 | **Revised:** 13 January 2025 | **Accepted:** 19 March 2025

Funding: This project was supported by the Deutsche Forschungsgemeinschaft (DFG, German Research Foundation) No. 441409627, as part of the PROSPAX consortium under the frame of EJP RD, the European Joint Programme on Rare Diseases, under the EJP RD COFUND-EJP No. 825575, the Fondazione Telethon and the Associazione ARSACS ODV - Italy (No. GSA21G005). FMS is partially supported by the Italian Ministry of Health, Ricerca Corrente 2024.

Keywords: ARSACS | ataxia | corticospinal tract | diffusion tensor imaging | magnetic resonance imaging

ABSTRACT

Background: Spasticity represents a core clinical feature of Autosomal Recessive Spastic Ataxia of Charlevoix-Saguenay (ARSACS) patients. Nonetheless, its pathophysiological substrate is poorly investigated. We assessed the microstructural integrity of the corticospinal tract (CST) using diffusion MRI (dMRI) via profilometry analysis to understand its possible role in the development of spasticity in ARSACS.

Abbreviations: ARSACS, Autosomal Recessive Spastic Ataxia of Charlevoix-Saguenay; CST, corticospinal tract; dMRI, diffusion MRI; MCP, middle cerebellar peduncles; SARA, Scale for the Assessment and Rating of Ataxia; SPAX, spastic ataxia; SPRS, Spastic Paraplegia Rating Scale; TPF, transverse pontine fibers; WM, white matter.

PROSPAX Consortium: Bernard Brais (Department of Neurology & Neurosurgery, Montreal Neurological Institute, McGill University, Montreal, Canada). Graziella Donatelli(Neuroradiology Unit, Azienda Ospedaliero-Universitaria Pisana, Pisa, Italy; Imago7 Research Foundation, Pisa, Italy) Giovanna De Michele (Department of Neurosciences and Reproductive and Odontostomatological Sciences, University of Naples "Federico II", Naples, Italy). Thomas M. Ernst (Department of Neurology and Center for Translational Neuro- and Behavioral Sciences (C-TNBS), Essen University Hospital, Essen, Germany). Stephan Klebe (Department of Neurology and Center for Translational Neuro- and Behavioral Sciences (C-TNBS), Essen University Hospital, Essen, Germany). Ilana Leppert (McConnell Brain Imaging Center, Montreal Neurological Institute, McGill University). Ivana Ricca (Department of Molecular Medicine, IRCCS Stella Maris Foundation, Pisa, Italy). Sara Satolli (Department of Molecular Medicine, IRCCS Stella Maris Foundation, Pisa, Italy). Andreas Traschütz (Division Translational Genomics of Neurodegenerative Diseases, Center for Neurology and Hertie Institute for Clinical Brain Research, University of Tübingen, Tübingen, Germany; German Center for Neurodegenerative Diseases (DZNE), Tübingen, Germany). Ilse Willemse (Department of Neurology, Radboud university medical center, Nijmegen, the Netherlands).

Materials and Methods: In this multi-center prospective study, data of 37 ARSACS (M/F = 21/16; 33.4 ± 12.4 years) and 29 controls (M/F = 13/16; 42.1 ± 17.2 years) acquired within the PROSPAX consortium were collected from January 2021 to October 2022 and analyzed. Differences in terms of global CST microstructural integrity were probed, as well as a possible spatial distribution of the damage along the tract via profilometry analysis. Possible correlations between clinical severity, including the Spastic Paraplegia Rating Scale (SPRS), were also tested.
Results: A significant global involvement of the CST was found in ARSACS compared to controls (all tests with $p < 0.001$), with a spatially defined pattern of more pronounced microstructural integrity loss occurring right below and above the pons, a structure that was also confirmed to be thickened in these patients ($p < 0.001$). A bilateral negative correlation emerged between the microstructural integrity of the CST and clinical indices of spasticity expressed via SPRS ($p = 0.02$ for both CSTs).
Conclusion: A clinically meaningful microstructural involvement of CST is present in ARSACS patients, with a spatially defined pattern of damage occurring right below and above a thickened pons. An evaluation of the microstructure of this bundle might serve as a possible biomarker in this condition.

1 | Introduction

Autosomal Recessive Spastic Ataxia of Charlevoix-Saguenay (ARSACS, MIM 270550) is an early-onset recessive form of spastic ataxia (SPAX), caused by mutations in the SACS gene [1]. First described in 1978 in French-Canadian families of Quebec, with a carrier frequency of 1/22 in the region of Charlevoix-Saguenay, ARSACS is now known to have a worldwide distribution, with more than a hundred disease-causing mutations identified to date [2].

The early onset of lower limbs spasticity with hyperreflexia represents a specific clinical feature of many ARSACS patients, becoming more evident when the patients start walking (usually between 12 and 24 months) [3, 4]. From a pathophysiological perspective, although being a complex phenomenon, spasticity [5] is sustained by an involvement of the upper motor neuron, and in turn of the corticospinal tract (CST) [6, 7]. The integrity of this structure can be explored in vivo using Magnetic Resonance Imaging (MRI), and in particular via diffusion MRI (dMRI), a technique that allows a non-invasive and accurate evaluation of white matter (WM) microstructural integrity [8]. Different metrics can be extracted from a single dMRI acquisition, all providing complementary information about tissue microstructure. To date, very few dMRI studies have been conducted to explore the presence of an involvement of the CST in ARSACS, and none have explored its correlation with patient clinical status. These few scattered studies have suggested a thinning of the CST in the pontine portion, also showing a lateral displacement, along with a possible increased number of latero-lateral oriented fibers in the pons [9, 10].

In the light of these evidences, it is therefore possible to hypothesize a gradient of damage affecting the CST arising from the pons to the cortex as one of the pathophysiological moments responsible, at least in part, for the development of clinical symptoms observed in these patients. Nonetheless, this hypothesis has never been tested to date, for different reasons ranging from the lack of relatively large and representative cohorts of patients with standardized imaging and clinical variables, as well as the lack of an appropriate methodology to properly test this hypothesis. In this study, we tried to overcome both these limitations by analyzing data acquired within an international multicenter collaborative research project, namely the PROSPAX consortium [11] and probe this possible gradient of microstructural damage of the CST using a relatively new data analysis technique called profilometry [12]. Furthermore, we also investigated the presence and the possible patterns of damage occurring at the level of the pontine fibers, anecdotally reported as thickened in this condition, as well as investigated the relevance of the microstructural CST damage observed in ARSACS patients by correlating dMRI metrics with clinical scores.

2 | Material and Methods

2.1 | Ethical Standards

Data analyzed in this study were acquired within the multi-center project PROSPAX ("An integrated multimodal progression chart in spastic ataxias"—ClinicalTrials.gov no:NCT04297891). The study was approved by local Ethics Committee of each center and written informed consent was obtained from each participant.

2.1.1 | Participants

In this prospective study, part of the multi-center project PROSPAX ("An integrated multimodal progression chart in spastic ataxias"—ClinicalTrials.gov no:NCT04297891), data of 197 subjects from 8 different world-wide centers from 6 countries were acquired from January 2021 to October 2022. These included 120 genetically confirmed ARSACS patients and 77 healthy controls (HC) without history of neurological or psychiatric disorders. Subjects with contraindication or unwillingness to undergo a brain MRI scan were excluded from the study, as well as subjects with a poor quality of the image or without a dMRI sequence and a T1-weighted volume acquired within the same MR session (Figure 1). For each subject, a neurologic examination was performed within 1 month from the MRI acquisition to assess the disease severity, via the Scale for the Assessment and Rating of Ataxia (SARA) [13] and the Spastic Paraplegia Rating Scale (SPRS) [14].

2.1.2 | MRI Data Acquisition

For each site, a standardized protocol on a 3 T scanner was acquired, including a high-resolution 3D-T1-weighted volume (voxel size $\leq 1\text{mm}^3$) acquired on a sagittal plane (see Supporting

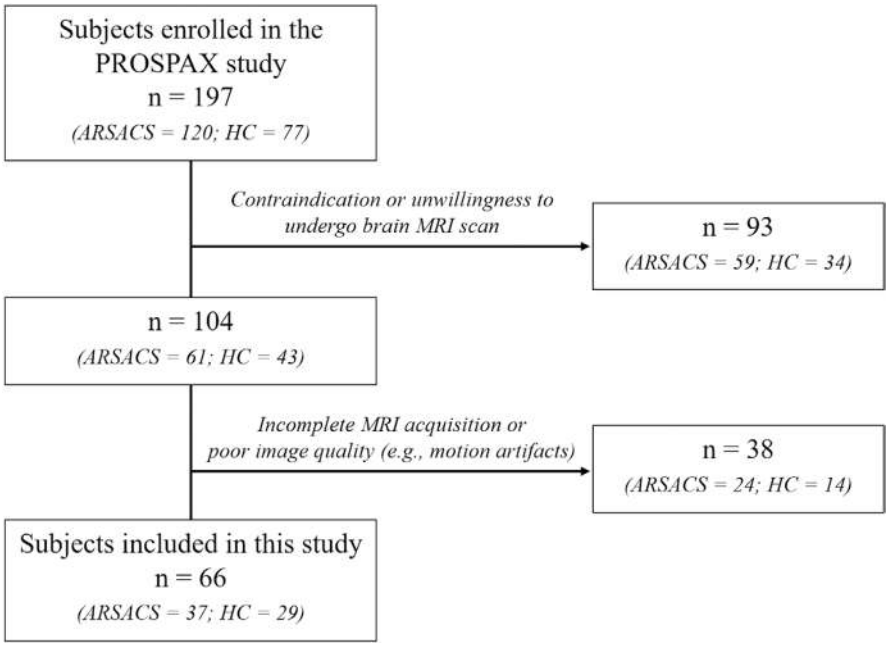

FIGURE 1 | Study flowchart. Flowchart showing how the final number of subjects analyzed in this study was reached after the application of inclusion and exclusion criteria. ARSACS = Autosomal Recessive Spastic Ataxia of Charlevoix-Saguenay, HC = healthy controls.

Information for a detailed list of the parameters) and a harmonized dMRI protocol (TR = 4200 ms; TE = 90 ms; flip angle = 90°; 72 axial slices; voxel size = $2 \times 2 \times 2\,mm^3$ with 3 directions at b = 300 s/mm^2, 6 directions at b = 700 s/mm^2, 32 directions at b = 1000 s/mm^2, 50 directions at b = 2000 s/mm^2 in addition to 7 directions at b = 0 s/mm^2; GRAPPA acceleration factor = 2; phase encoding = AP; bandwidth = 1780 Hz/pixel), followed by another acquisition with an inverse phase encoding direction (PA) and 3 directions at b = 0 s/mm^2 values, used for distortion correction purposes.

A complete list of all the scanners used at each site included in the analysis is available in Supporting Information.

2.1.3 | MRI Data Processing

The 3D-T1-weighted images were segmented into five distinct volumes (WM, gray matter-GM-, sub-cortical GM, cerebrospinal fluid, and potential pathological tissue) using the MRtrix3 [15] command *5ttgen* [16] and the *fsl* algorithm, resulting in the creation of a mask representing the white matter-gray matter (WM-GM) interface. The cortical and subcortical structures were parcellated into 85 regions of interest using FreeSurfer 6.0 (https://freesurfer.net) [17] according to the Desikan-Killiany atlas [18]. Then, these ROIs were co-registered, along with the T1-weighted volume, the segmentation output of the *5ttgen* command, and the corresponding WM-GM interface mask, in the subject-specific dMRI space using *FMRIB's Linear Image Registration Tool* (FLIRT) [19], with boundary-based cost function and nearest-neighbor interpolation.

All dMRI images underwent denoising [20, 21] and preprocessing using the FMRIB Software Library (FSL version 6.0) toolbox (http://www.fmrib.ox.ac.uk/fsl), incorporating the *eddy* and *topup* distortion correction commands [22–24]. The fiber orientation distribution (FOD) functions were determined through multi-shell multi-tissue constrained spherical deconvolution [25]. Then, the probabilistic algorithm *iFOD2* [26] was used to generate 1 million streamlines interrupting as they crossed the GM-WM interface mask, using the Anatomically Constrained Tractography (ACT) during tracking [16] with the following settings: cutoff value = 0.05, maximum and minimum length of the tracks = 250 and 5, respectively, maximum angle in degrees between successive steps = 30.

For each subject, the diffusion tensor model was fitted using b ≤ 1000 s/mm^2 data [27]. Fractional Anisotropy (FA), Mean Diffusivity (MD), and Radial Diffusivity (RD) maps were computed from this model [28]. Since the direction of Axial Diffusivity (AD) may not be preserved in the presence of pathological tissue, potentially causing it to deviate from the underlying tissue structure, as can be seen in regions with low anisotropy, in voxels affected by partial volume, and in areas where crossed fibers are present, AD was excluded from the

TABLE 1 | Demographic and clinical data of the subjects included in this study.

	ARSACS ($n = 37$)	HC ($n = 29$)	p
Age	34 [16–63]	41 [17–77]	0.04
Sex (M/F)	21/16	13/16	0.47
AAO	6.9 ± 7.9	n.a.	n.a.
SARA	16 [4–33]	0 [0–4]	< 0.001
SPRS	24 [6–39]	0 [0–5]	< 0.001

Note: Age at onset is reported as mean and standard deviation, while age and clinical scores are reported as median values, with corresponding ranges in brackets.
Abbreviations: AAO = Age at onset, ARSACS = Autosomal Recessive Spastic Ataxia of Charlevoix-Saguenay, HC = healthy controls, SARA = Scale for the Assessment and Rating of Ataxia, SPRS = Spastic Paraplegia Rating Scale.

analyses [29–31]. Additionally, a Neurite Orientation Dispersion and Density Imaging (NODDI) model [32] was also fitted using AMICO (Accelerated Microstructure Imaging via Convex Optimization [33]). From this analysis, the corresponding neurite density index (NDI_w) maps, weighted by the tissue fraction [34], were obtained as a putative marker of neurites.

Finally, although all images were acquired using the same standardized acquisition protocol, to remove any possible residual variance caused by scanner and site differences, the *ComBat* data harmonization method (https://github.com/Jfortin1/ComBatHarmonization [35]) was applied to the derived microstructural maps.

2.1.4 | MRI Data Analysis

To retrieve the pontine fibers volume, first we used the segmentation output of FreeSurfer [36] to identify the regions, and then the corresponding fibers were extracted using MRtrix3.

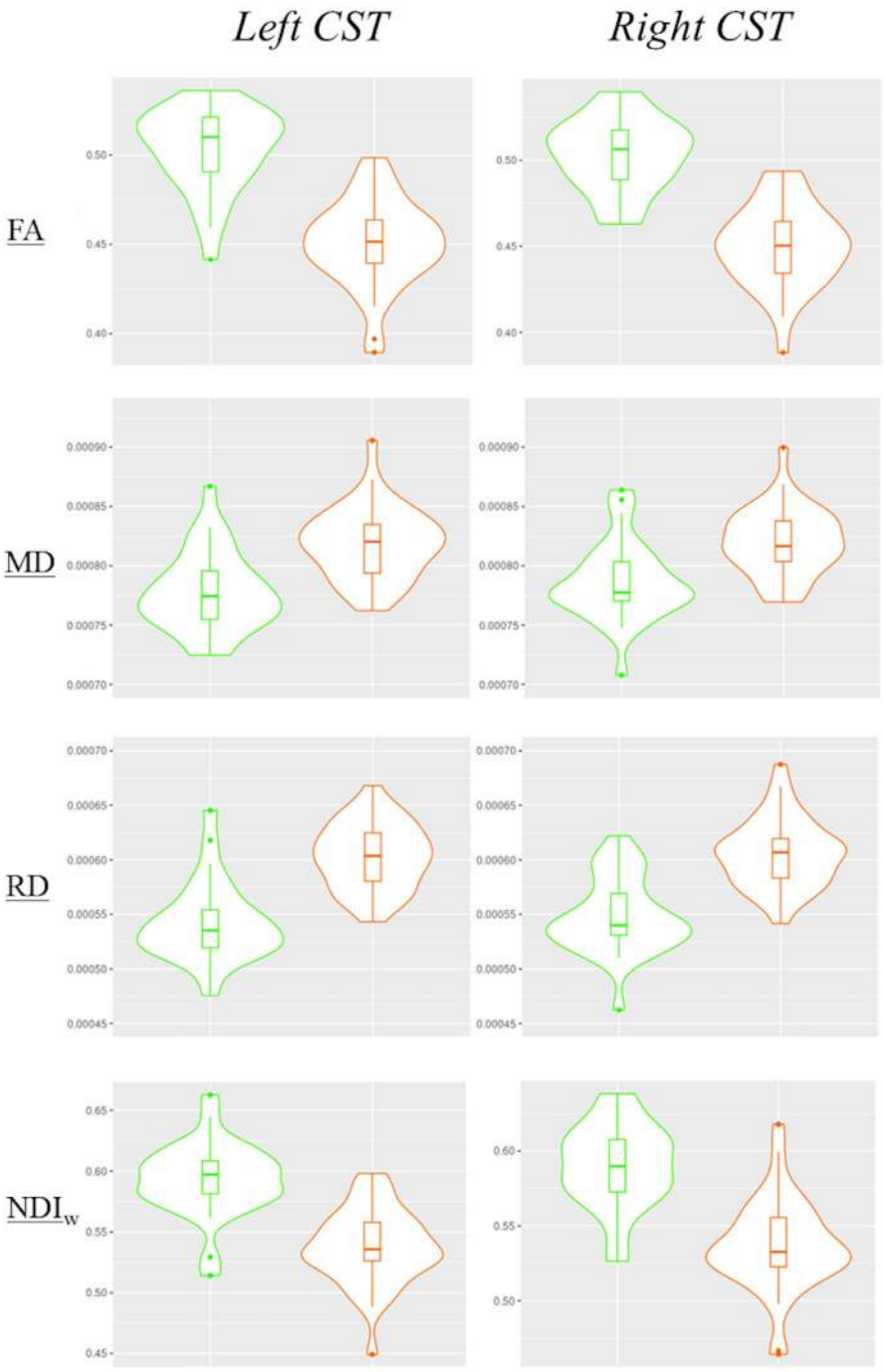

FIGURE 2 | Differences between groups in terms of mean microstructure of the CST. Violin plots showing the differences between ARSACS (*orange*) and HC (*green*) in terms of CST mean microstructural metrics. ARSACS = Autosomal Recessive Spastic Ataxia of Charlevoix-Saguenay, CST = corticospinal tract, FA = fractional anisotropy, HC = healthy controls, MD = mean diffusivity, RD = radial diffusivity, NDI_w = neurite density index.

Then, to extract the transverse pontine fibers (TPF) portion from the other fibers that are part of the pons, the following procedure was performed. Using a WM atlas [37] we divided the pons into two portions: a first one including fibers encompassing the middle cerebellar peduncles (MCP) and a second one representing the remaining fibers, and therefore the TPF. Reconstructed fibers were then mapped into the corresponding images, and the three fiber volumes (total pontine fibers volume, and the corresponding TFP and MCP portions) were extracted and divided by the total WM volume for normalization procedure.

Using *The White Matter Query Language* (WMQL) technique [38], left and right CST were identified from the whole brain tractograms, with the *RecoBundles* approach that was used to improve their quality [39]. To minimize possible errors in fascicle identification due to their physiological decussation, CST bundles lower limit was defined right above the medullary pyramids. The streamlines were clustered using QuickBundles [40], choosing as statistics the average point-wise Euclidean metric from FA, MD, and RD volumes. Finally, left and right CST profiles were extracted using the *DiPy* pipeline (https://dipy.org/index.html) and resampled within 100 points for the profilometry analysis.

All procedure steps were revised case by case and step by step by an expert reader to ensure a good quality of the processing outcomes.

2.2 | Statistical Analysis

Unless otherwise specified, all analyses were performed using the RStudio software (R Core Team 2022- https://www.R-project.org/), with a significance level set for $p < 0.05$.

2.2.1 | Between Group Differences—Demographics

Possible differences between patients and controls in terms of sex and age were tested via a Pearson's Chi-squared test and a Wilcoxon rank sum test, respectively.

2.2.2 | Between Group Differences—Pontine and Tractometry-Based Data

Between-groups differences in terms of global pontine volume, as well as the sub-analysis evaluating possible differences in TPF and corresponding MCP portion of the pons, were carried out via a robust linear regression model, considering age and sex as covariates.

Between-groups differences in terms of global CST microstructural integrity were tested via a tractometry-based technique, sampling the values of the microstructural images along the tracks, and retrieving their mean using MRtrix3. Similarly to the pontine analysis, this possible difference between ARSACS and HC was also probed via a robust linear regression model age and sex corrected.

2.2.3 | Between Group Differences—Profilometry Analysis

Between-group microstructural differences along the CST were tested using *TractSeg* [41], with age and sex added in the analysis as covariates.

2.2.4 | Correlation With Clinical Data

Possible correlation between the clinical scores (SARA and SPRS scores, as indices of the ataxic and the spastic components of the disease, respectively) and the FA values (as index of CST's microstructural involvement [42, 43]) was tested by evaluating the possible relation with the mean FA value along the entire tract (via robust linear regression model, considering age and sex as covariates) and using a profilometry approach via TractSeg and its "target" option [41, 44, 45], with both analyses corrected for age and sex.

3 | Results

After applying the exclusion criteria, a final number of 66 subjects from 5 sites were included in this study (Figure 1), with MRI data of 37 ARSACS patients (M/F = 21/16, 33.4 ± 12.4) and 29 HC (M/F = 13/16, 42.1 ± 17.2) that were analyzed. Demographic and clinical data of the subjects involved in this study are shown in Table 1.

When evaluating possible differences in terms of pontine volumes between ARSACS and HC, an increased volume of the pons was found in ARSACS subjects (0.017 ± 0.002 vs. 0.014 ± 0.002 mm^3, $p < 0.001$). Interestingly, when the pontine volume was divided into the TPF component and the corresponding MCP portions, the observed increase in volume was mainly due to the latter component (0.017 ± 0.002 vs. 0.014 ± 0.002, $p < 0.001$), with a reduction of the TPF (0.00218 ± 0.0007 vs. 0.0031 ± 0.0008, $p < 0.001$).

TABLE 2 | Results of the mean microstructural analysis of the CST.

	ARSACS	HC	*p*
FA–Left CST	0.45 ± 0.02	0.50 ± 0.02	< 0.001
FA–Right CST	0.45 ± 0.02	0.50 ± 0.02	< 0.001
MD–Left CST	0.82 ± 0.030	0.78 ± 0.030	< 0.001
MD–Right CST	0.82 ± 0.028	0.79 ± 0.033	< 0.001
RD–Left CST	0.61 ± 0.034	0.54 ± 0.036	< 0.001
RD–Right CST	0.61 ± 0.031	0.55 ± 0.035	< 0.001
NDI_w–Left CST	0.54 ± 0.03	0.59 ± 0.03	< 0.001
NDI_w–Right CST	0.54 ± 0.03	0.59 ± 0.03	< 0.001

Note: MD and RD maps' values are reported in 10^{-3} mm^2/s, while FA and NDI_w are adimensional. All values are expressed as mean and standard deviation.
Abbreviations: ARSACS = Autosomal Recessive Spastic Ataxia of Charlevoix-Saguenay, CST = corticospinal tract, FA = fractional anisotropy, HC = healthy controls, MD = mean diffusivity, NDI_w = neurite density index, RD = radial diffusivity.

When assessing potential differences between the two groups in terms of mean microstructure of the CST, ARSACS patients showed a significant involvement of this bundle compared to controls, depicted by a global reduction in FA and NDI_w values for both left and right CST bundles, coupled with an increase in MD and RD (all with $p < 0.001$). A graphical representation of these results is available in Figure 2, with the corresponding values that are reported in Table 2.

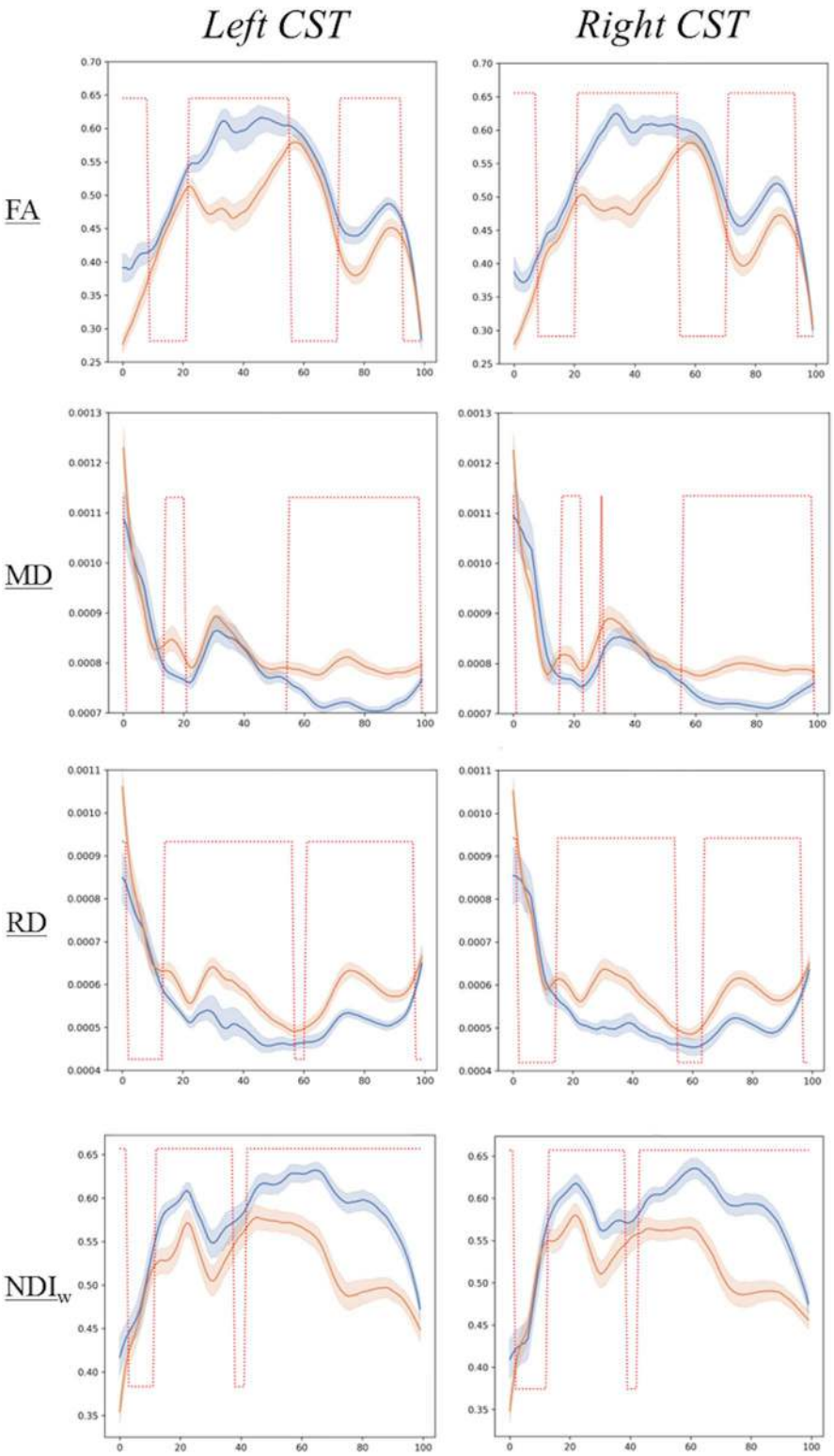

FIGURE 3 | Results of the profilometry analysis. Results of the profilometry analysis showing the spatial distribution of microstructural damage along the CST (*x-axis, ranging from 0-pyramids- to 100-cortex*) in ARSACS (*orange lines*) and HC (*blue lines*). Red lines indicate where, along the CST, significant differences between groups occurs. ARSACS = Autosomal Recessive Spastic Ataxia of Charlevoix-Saguenay, CST = corticospinal tract, FA = fractional anisotropy, HC = healthy controls, MD = mean diffusivity, RD = radial diffusivity, NDI_w = neurite density index.

The spatial distribution of this widespread damage along the CST was then probed via profilometry analysis, showing the occurrence of a gradient of microstructural damage (depicted via the evaluation of FA) with a more pronounced reduction of this metric affecting the CST right above and below the pons, and in particular at the level of midbrain, the cerebral peduncles, and the posterior limb of internal capsule (PLIC), with less significant changes affecting the bundle portion closer to the cortex. A similar, although more extended, pattern of damage was found when RD was evaluated, while MD and NDI_w changes were more pronounced in the final portion of the tract compared to the findings observed in FA and RD. Plots showing the results of the profilometry analysis are shown in Figure 3, while a graphical representation of the localization and the degree of CST microstructural damage (expressed by FA) according to the Cohen-d values is shown in Figure 4.

Finally, the analysis probing the possible clinical counterpart of the observed microstructural changes showed that, when evaluating the mean microstructural status of the CST, no significant correlation with either the left or right CST with SARA ($\rho = 0.10$, $p = 0.35$, Figure 5A) and SPRS ($\rho = 0.65$, $p = 0.68$, Figure 5A) was found. Interestingly, when the profilometry approach was performed, a spatially defined bilateral negative correlation emerged between the microstructural integrity of the CST portion above the pons and clinical indices of spasticity expressed by SPRS score ($p = 0.023$ and $p = 0.021$ for left and right CST respectively, Figure 5B), while a significant correlation with SARA was found only for the left CST ($p = 0.002$, Figure 5B), approaching but not reaching the significance threshold on the right bundle ($p = 0.07$, Figure 5B).

4 | Discussion

In this study, we investigated the microstructural integrity of the CST to assess a possible specific gradient of its damage in a large sample of ARSACS patients, hypothesizing the occurrence of greater damage of these fibers at the level of the pons, showing a gradient of reduction moving towards the cortex.

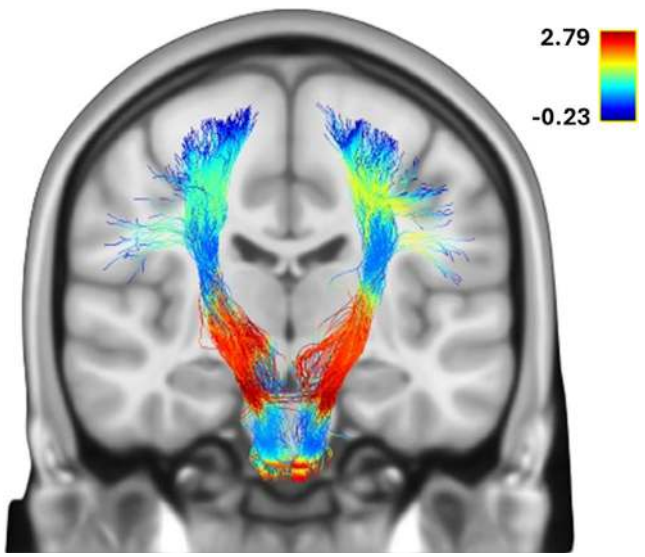

FIGURE 4 | Localization and the degree of CST microstructural damage. Representation of the spatial profile and magnitude of microstructural damage affecting the CST using a color-coded scale weighted by Cohen-d values. CST = corticospinal tract.

The rationale behind this study derives from the clinical observation of spasticity, an undoubted core feature of this condition linked to the integrity of the CST, as well as from the few dMRI reports on small groups of patients suggesting an alteration of this bundle at the level of the pons. In particular, an apparent increased number of pontocerebellar fibers, as well as a thickening of the TPF, have been reported in ARSACS, possibly resulting in a CST compression at its pontine level [9, 10, 46]. In line with these previous studies, we found that ARSACS patients show indeed an overall increase in pontine fibers. Nonetheless, the major contributor to this pontine thickening proved to be, rather than a "pure" hypertrophy of the TPF (which were reduced in our sample compared to HC), a greater representation of the MCP fibers contributing to the pons. Previous studies have proposed a neurodevelopmental hypothesis in ARSACS patients to explain the finding of a thickened pons in this condition, suggesting a primary developmental alteration of the pontocerebellar fibers, followed by a secondary degenerative process of the superior vermis cortex sustained by a glutamate excitotoxicity [9, 46]. Our results do not allow us to exclude this hypothesis, which seems reasonable although worthy of confirmation with studies including pediatric patients and/or pre-clinical models. Furthermore, they also expand the current knowledge by showing that if a neurodevelopmental change would occur, this might be at the level of the main cerebellar afferences (namely, the MCP) rather than the intra-pontine fibers.

Along with changes in pontine structure, previous studies either qualitatively evaluated the damage affecting the CST or used a voxel-wise approach that, although providing insightful information, shows an intrinsic limited anatomical specificity [47]. Here we tried to overcome these limitations by applying a profilometry approach, a technique particularly suited for the hypothesis here tested, given that it allows studying the spatial distribution of microstructural damage along a specific tract [48]. Our results showed that indeed in ARSACS patients is present not only a global involvement of this bundle, but a gradient of microstructural damage affecting the CST, with the most affected regions being located just below and above the pons, with a reducing gradient of damage closer to the cortex. The advantage of this approach was also proven by the results of the correlation with clinical data, where a "conventional" correlation between mean microstructural integrity and clinical scores hindered significant associations, which were found to be spatially localized in specific portions of the CST via profilometry analysis.

Interestingly, while we found significant microstructural changes affecting the CST in its medulla oblongata portion, as well as at the level of midbrain, cerebral peduncles, and PLIC, we failed to find significant differences at the level of the pontine portion of the CST. This result, counterintuitive and apparently advising against our hypothesis, can nonetheless be explained by a methodological reason intrinsic to the dMRI technique itself. In particular, it is possible to hypothesize that the lack of difference between HC and ARSACS for CST microstructural

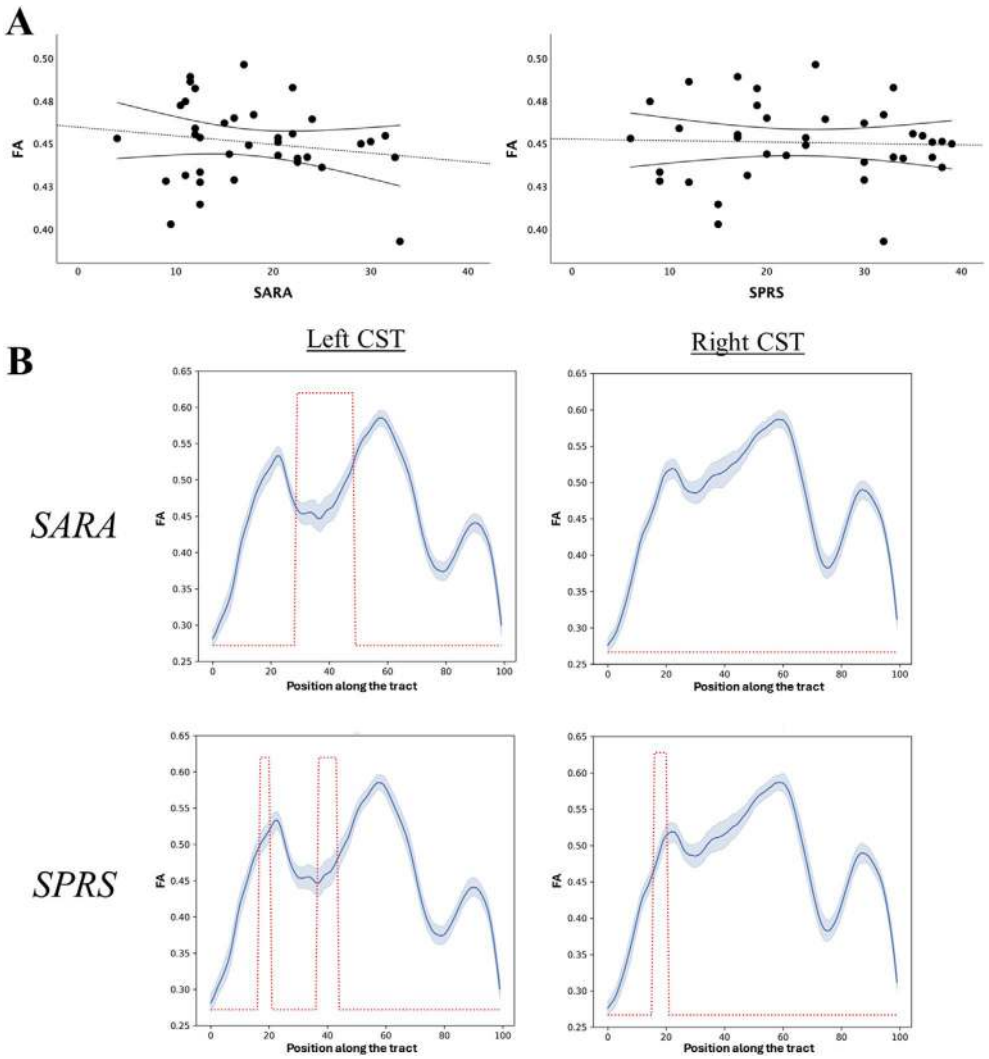

FIGURE 5 | Results of the correlation analyses between microstructural changes and clinical scores in ARSACS. In (A), scatterplots of the correlation analyses between mean FA value along the entire CST (y-axes) and SARA (*left*) and SPRS (*right*) scores (*x-axes*) showing the absence of a significant correlation when this approach was used. In (B) results of the correlation analyses using a profilometry approach between FA values along the CST of ARSACS subjects and SARA (*upper row*) and SPRS scores (*lower row*) showing the occurrence of a significant and spatially distributed correlation between CST microstructure and clinical scores. Red lines indicate significant correlations between the microstructural damage and the corresponding clinical variable along the CST (*x-axis, ranging from 0-pyramids- to 100-cortex*). ARSACS = Autosomal Recessive Spastic Ataxia of Charlevoix-Saguenay, CST = corticospinal tract, FA = fractional anisotropy, SARA = Scale for the Assessment and Rating of Ataxia, SPRS = Spastic Paraplegia Rating Scale.

variables (i.e., FA) could be the result of a simultaneous expected reduction of this metric (i.e., following the neuronal changes occurring in ARSACS) coupled to an apparent increase. This latter phenomenon can indeed be observed in those cases where crossing fibers are present, and a disproportionate damage of one bundle (i.e., the CST in this case) over the remaining fibers could lead to a paradoxical increase in FA, despite an actual net decrease in local fiber density and/or myelination [49]. Furthermore, the paradoxical absence of FA changes in the pons area has also been described in subjects with Wallerian degeneration of the CST following vascular damage at the level of the PLIC, as fibers are more coherently oriented within the voxel following the damage of this WM tract [50].

Along with changes in FA, we also found modifications of the other investigated microstructural maps (namely, MD, RD and NDI_w) in ARSACS compared to HC. Of particular interest are the results obtained by RD maps, as this metric has been long hypothesized to be a putative marker of demyelination. The occurrence of myelin changes along the axons of ARSACS patients is getting increasing interest in the scientific community, with the very recent evidence of a possible pattern of peripheral demyelination [51] that is in line with older neuropathological data, showing a demyelination along the CST in the medulla and spinal cord of these patients [52]. It is noteworthy to mention that these latter changes were significantly marked in the upper cervical cord, a region reported to be affected by a prominent reduction in volume at a qualitative evaluation of brain images [53]. Although the CST damage below the level of the pons was only partly analyzed in this study, we can only speculate on the occurrence also of a gradient of anterograde damage directed to the cervical cord.

For this reason, future studies evaluating spinal cord microstructure are warranted to evaluate a possible downward gradient of the damage affecting the CST, and further understand the exact degree of involvement of this region.

Additional limitations of this study should be mentioned. In particular, although being widely recognized as one of (if not the) techniques to evaluate microstructure, dMRI shows different limitations, some of which have been previously described. Other techniques (such as Myelin Water Fraction or Magnetization Transfer Ratio) can be used to evaluate microstructure, possibly providing additional information that might be only partly obtained via dMRI. Another limitation lies in the cross-sectional nature of this study, which does not allow us to obtain information about possible changes over time of both pontine thickening and CST microstructural changes. Nonetheless, these limitations are balanced by the evaluation of a large group of patients, with a high-quality standardized MRI and clinical protocol.

In conclusion, in this study we were able to confirm the occurrence of a thickened pons in ARSACS, mainly attributable to an increase of the MCP and the corresponding pontine projections rather than a "pure" thickening of the TPF. Furthermore, and most importantly, we demonstrated the occurrence of a clinically meaningful ascending gradient of microstructural damage affecting the CST that might explain the observed spastic phenotype in these patients and might serve as a potential biomarker to evaluate disease progression and, in future, possible therapeutic interventions.

Author Contributions

Alessandra Scaravilli: writing – original draft, data curation, investigation, formal analysis. **Gaia Mari:** writing – review and editing, formal analysis, data curation, software, investigation. **Ilaria Gabusi:** writing – review and editing, formal analysis, data curation, software, investigation. **Matteo Battocchio:** writing – review and editing, formal analysis, data curation, software, investigation. **Sara Bosticardo:** writing – review and editing, formal analysis, data curation, software, investigation. **Simona Schiavi:** writing – review and editing, formal analysis, data curation, software, investigation. **Benjamin Bender:** writing – review and editing, project administration, data curation. **Christoph Kessler:** writing – review and editing, project administration, data curation. **Roberta La Piana:** writing – review and editing, project administration, data curation. **Bart P. van de Warrenburg:** writing – review and editing, project administration, data curation. **Mirco Cosottini:** writing – review and editing, project administration, data curation. **Dagmar Timmann:** writing – review and editing, project administration, data curation. **Alessandro Daducci:** writing – review and editing, formal analysis, conceptualization, project administration, software. **Rebecca Schüle:** writing – review and editing, conceptualization, project administration. **Matthis Synofzik:** writing – review and editing, conceptualization, project administration. **Filippo Maria Santorelli:** writing – review and editing, supervision, conceptualization, project administration, data curation. **Sirio Cocozza:** writing – original draft, writing – review and editing, supervision, formal analysis, conceptualization, data curation, software, investigation.

Acknowledgements

This project was supported by the Deutsche Forschungsgemeinschaft (DFG, German Research Foundation) No. 441409627, as part of the PROSPAX consortium under the frame of EJP RD, the European Joint Programme on Rare Diseases, under the EJP RD COFUND-EJP No. 825575, the Fondazione Telethon and the Associazione ARSACS ODV - Italy (No. GSA21G005). FMS is partially supported by the Italian Ministry of Health, Ricerca Corrente 2024. Open access funding provided by BIBLIOSAN. Bernard Brais, Graziella Donatelli, Giovanna De Michele, Thomas M. Ernst, Stephan Klebe, Ilana Leppert, Ivana Ricca, Sara Satolli, Andreas Traschütz, Ilse Willemse,

Conflicts of Interest

S.C. have received fees for Advisory Board by Amicus. All other coauthors declare no conflicts of interest.

Data Availability Statement

The data that support the findings of this study are available from the corresponding author upon reasonable request.

References

1. J. C. Engert, P. Bérubé, J. Mercier, et al., "ARSACS, a Spastic Ataxia Common in Northeastern Québec, Is Caused by Mutations in a New Gene Encoding an 11.5-Kb ORF," *Nature Genetics* 24, no. 2 (2000): 120–125, https://doi.org/10.1038/72769.

2. J. Baets, T. Deconinck, K. Smets, et al., "Mutations in *SACS* Cause Atypical and Late-Onset Forms of ARSACS," *Neurology* 75, no. 13 (2010): 1181–1188, https://doi.org/10.1212/WNL.0b013e3181f4d86c.

3. B. L. Fogel and S. Perlman, "Clinical Features and Molecular Genetics of Autosomal Recessive Cerebellar Ataxias," *Lancet Neurology* 6, no. 3 (2007): 245–257, https://doi.org/10.1016/S1474-4422(07)70054-6.

4. Y. Bouhlal, R. Amouri, G. El Euch-Fayeche, and F. Hentati, "Autosomal Recessive Spastic Ataxia of Charlevoix–Saguenay: An Overview," *Parkinsonism & Related Disorders* 17, no. 6 (2011): 418–422, https://doi.org/10.1016/j.parkreldis.2011.03.005.

5. S. Vermeer, R. P. P. Meijer, B. J. Pijl, et al., "ARSACS in the Dutch Population: A Frequent Cause of Early-Onset Cerebellar Ataxia," *Neurogenetics* 9, no. 3 (2008): 207–214, https://doi.org/10.1007/s10048-008-0131-7.

6. C. Trompetto, L. Marinelli, L. Mori, et al., "Pathophysiology of Spasticity: Implications for Neurorehabilitation," *BioMed Research International* 2014 (2014): 354906, https://doi.org/10.1155/2014/354906.

7. A. Mukherjee and A. Chakravarty, "Spasticity Mechanisms – For the Clinician," *Frontiers in Neurology* 1 (2010): 149, https://doi.org/10.3389/fneur.2010.00149.

8. Y. Assaf and O. Pasternak, "Diffusion Tensor Imaging (DTI)-Based White Matter Mapping in Brain Research: A Review," *Journal of Molecular Neuroscience* 34, no. 1 (2008): 51–61, https://doi.org/10.1007/s12031-007-0029-0.

9. J. Gazulla, A. C. Vela, M. A. Marín, et al., "Is the Ataxia of Charlevoix–Saguenay a Developmental Disease?," *Medical Hypotheses* 77, no. 3 (2011): 347–352, https://doi.org/10.1016/j.mehy.2011.05.011.

10. K. K. Oguz, G. Haliloglu, C. Temucin, et al., "Assessment of Whole-Brain White Matter by DTI in Autosomal Recessive Spastic Ataxia of Charlevoix-Saguenay," *AJNR. American Journal of Neuroradiology* 34, no. 10 (2013): 1952–1957, https://doi.org/10.3174/ajnr.A3488.

11. "PROSPAX—An Integrated Multimodal Progression Chart in Spastic Ataxias. PROSPAX,", https://www.prospax.net/.

12. M. Dayan, E. Monohan, S. Pandya, et al., "Profilometry: A New Statistical Framework for the Characterization of White Matter Pathways, With Application to Multiple Sclerosis," *Human Brain Mapping* 37, no. 3 (2016): 989–1004, https://doi.org/10.1002/hbm.23082.

13. T. Schmitz-Hübsch, S. T. Du Montcel, L. Baliko, et al., "Scale for the Assessment and Rating of Ataxia: Development of a New Clinical

Scale," *Neurology* 66, no. 11 (2006): 1717–1720, https://doi.org/10.1212/01.wnl.0000219042.60538.92.

14. R. Schule, T. Holland-Letz, S. Klimpe, et al., "The Spastic Paraplegia Rating Scale (SPRS): A Reliable and Valid Measure of Disease Severity," *Neurology* 67, no. 3 (2006): 430–434, https://doi.org/10.1212/01.wnl.0000228242.53336.90.

15. J. D. Tournier, R. Smith, D. Raffelt, et al., "MRtrix3: A Fast, Flexible and Open Software Framework for Medical Image Processing and Visualisation," *NeuroImage* 202 (2019): 116137, https://doi.org/10.1016/j.neuroimage.2019.116137.

16. R. E. Smith, J. D. Tournier, F. Calamante, and A. Connelly, "Anatomically-Constrained Tractography: Improved Diffusion MRI Streamlines Tractography Through Effective Use of Anatomical Information," *NeuroImage* 62, no. 3 (2012): 1924–1938, https://doi.org/10.1016/j.neuroimage.2012.06.005.

17. B. Fischl, "FreeSurfer," *NeuroImage* 62, no. 2 (2012): 774–781, https://doi.org/10.1016/j.neuroimage.2012.01.021.

18. R. S. Desikan, F. Ségonne, B. Fischl, et al., "An Automated Labeling System for Subdividing the Human Cerebral Cortex on MRI Scans Into Gyral Based Regions of Interest," *NeuroImage* 31, no. 3 (2006): 968–980, https://doi.org/10.1016/j.neuroimage.2006.01.021.

19. M. Jenkinson, P. Bannister, M. Brady, and S. Smith, "Improved Optimization for the Robust and Accurate Linear Registration and Motion Correction of Brain Images," *NeuroImage* 17, no. 2 (2002): 825–841, https://doi.org/10.1006/nimg.2002.1132.

20. J. Veraart, D. S. Novikov, D. Christiaens, B. Ades-Aron, J. Sijbers, and E. Fieremans, "Denoising of Diffusion MRI Using Random Matrix Theory," *NeuroImage* 142 (2016): 394–406, https://doi.org/10.1016/j.neuroimage.2016.08.016.

21. J. Veraart, E. Fieremans, and D. S. Novikov, "Diffusion MRI Noise Mapping Using Random Matrix Theory," *Magnetic Resonance in Medicine* 76, no. 5 (2016): 1582–1593, https://doi.org/10.1002/mrm.26059.

22. E. Gibbs and C. Liu, "Feasibility of Imaging Tissue Electrical Conductivity by Switching Field Gradients With MRI," *Tomography* 1, no. 2 (2015): 125–135, https://doi.org/10.18383/j.tom.2015.00142.

23. M. A. Horsfield, "Mapping Eddy Current Induced Fields for the Correction of Diffusion-Weighted Echo Planar Images," *Magnetic Resonance Imaging* 17, no. 9 (1999): 1335–1345, https://doi.org/10.1016/S0730-725X(99)00077-6.

24. H. Yamada, O. Abe, T. Shizukuishi, et al., "Efficacy of Distortion Correction on Diffusion Imaging: Comparison of FSL Eddy and Eddy_Correct Using 30 and 60 Directions Diffusion Encoding," *PLoS One* 9, no. 11 (2014): e112411, https://doi.org/10.1371/journal.pone.0112411.

25. B. Jeurissen, J. D. Tournier, T. Dhollander, A. Connelly, and J. Sijbers, "Multi-Tissue Constrained Spherical Deconvolution for Improved Analysis of Multi-Shell Diffusion MRI Data," *NeuroImage* 103 (2014): 411–426, https://doi.org/10.1016/j.neuroimage.2014.07.061.

26. J. Tournier, F. Calamante, and A. Connelly, "MRtrix: Diffusion Tractography in Crossing Fiber Regions," *International Journal of Imaging Systems and Technology* 22, no. 1 (2012): 53–66, https://doi.org/10.1002/ima.22005.

27. L. J. O'Donnell and C. F. Westin, "An Introduction to Diffusion Tensor Image Analysis," *Neurosurgery Clinics of North America* 22, no. 2 (2011): 185–196, https://doi.org/10.1016/j.nec.2010.12.004.

28. D. Le Bihan, J. Mangin, C. Poupon, et al., "Diffusion Tensor Imaging: Concepts and Applications," *Magnetic Resonance Imaging* 13, no. 4 (2001): 534–546, https://doi.org/10.1002/jmri.1076.

29. Y. You, C. Joseph, C. Wang, et al., "Demyelination Precedes Axonal Loss in the Transneuronal Spread of Human Neurodegenerative Disease," *Brain* 142, no. 2 (2019): 426–442, https://doi.org/10.1093/brain/awy338.

30. S. Schiavi, M. Petracca, P. Sun, et al., "Non-Invasive Quantification of Inflammation, Axonal and Myelin Injury in Multiple Sclerosis," *Brain* 144, no. 1 (2021): 213–223, https://doi.org/10.1093/brain/awaa381.

31. C. A. M. Wheeler-Kingshott and M. Cercignani, "About "Axial" and "Radial" Diffusivities," *Magnetic Resonance in Medicine* 61, no. 5 (2009): 1255–1260, https://doi.org/10.1002/mrm.21965.

32. H. Zhang, T. Schneider, C. A. Wheeler-Kingshott, and D. C. Alexander, "NODDI: Practical In Vivo Neurite Orientation Dispersion and Density Imaging of the Human Brain," *NeuroImage* 61, no. 4 (2012): 1000–1016, https://doi.org/10.1016/j.neuroimage.2012.03.072.

33. A. Daducci, E. J. Canales-Rodríguez, H. Zhang, T. B. Dyrby, D. C. Alexander, and J. P. Thiran, "Accelerated Microstructure Imaging via Convex Optimization (AMICO) From Diffusion MRI Data," *NeuroImage* 105 (2015): 32–44, https://doi.org/10.1016/j.neuroimage.2014.10.026.

34. C. S. Parker, T. Veale, M. Bocchetta, et al., "Not all Voxels Are Created Equal: Reducing Estimation Bias in Regional NODDI Metrics Using Tissue-Weighted Means," *NeuroImage* 245 (2021): 118749, https://doi.org/10.1016/j.neuroimage.2021.118749.

35. J. P. Fortin, D. Parker, B. Tunç, et al., "Harmonization of Multi-Site Diffusion Tensor Imaging Data," *NeuroImage* 161 (2017): 149–170, https://doi.org/10.1016/j.neuroimage.2017.08.047.

36. J. E. Iglesias, K. Van Leemput, P. Bhatt, et al., "Bayesian Segmentation of Brainstem Structures in MRI," *NeuroImage* 113 (2015): 184–195, https://doi.org/10.1016/j.neuroimage.2015.02.065.

37. K. M. Van Baarsen, M. Kleinnijenhuis, S. Jbabdi, S. N. Sotiropoulos, J. A. Grotenhuis, and A. M. Van Cappellen Walsum, "A Probabilistic Atlas of the Cerebellar White Matter," *NeuroImage* 124 (2016): 724–732, https://doi.org/10.1016/j.neuroimage.2015.09.014.

38. D. Wassermann, N. Makris, Y. Rathi, et al., "The White Matter Query Language: A Novel Approach for Describing Human White Matter Anatomy," *Brain Structure & Function* 221, no. 9 (2016): 4705–4721, https://doi.org/10.1007/s00429-015-1179-4.

39. E. Garyfallidis, M. A. Côté, F. Rheault, et al., "Recognition of White Matter Bundles Using Local and Global Streamline-Based Registration and Clustering," *NeuroImage* 170 (2018): 283–295, https://doi.org/10.1016/j.neuroimage.2017.07.015.

40. E. Garyfallidis, M. Brett, M. M. Correia, G. B. Williams, and I. Nimmo-Smith, "QuickBundles, a Method for Tractography Simplification," *Frontiers in Neuroscience* 6 (2012): 175, https://doi.org/10.3389/fnins.2012.00175.

41. B. Q. Chandio, S. L. Risacher, F. Pestilli, et al., "Bundle Analytics, a Computational Framework for Investigating the Shapes and Profiles of Brain Pathways Across Populations," *Scientific Reports* 10, no. 1 (2020): 17149, https://doi.org/10.1038/s41598-020-74054-4.

42. W. S. Tae, B. J. Ham, S. B. Pyun, S. H. Kang, and B. J. Kim, "Current Clinical Applications of Diffusion-Tensor Imaging in Neurological Disorders," *Journal of Clinical Neurology* 14, no. 2 (2018): 129, https://doi.org/10.3988/jcn.2018.14.2.129.

43. A. Lerner, M. A. Mogensen, P. E. Kim, M. S. Shiroishi, D. H. Hwang, and M. Law, "Clinical Applications of Diffusion Tensor Imaging," *World Neurosurgery* 82, no. 1–2 (2014): 96–109, https://doi.org/10.1016/j.wneu.2013.07.083.

44. J. Wasserthal, K. H. Maier-Hein, P. F. Neher, et al., "Multiparametric Mapping of White Matter Microstructure in Catatonia," *Neuropsychopharmacology* 45, no. 10 (2020): 1750–1757, https://doi.org/10.1038/s41386-020-0691-2.

45. J. D. Yeatman, R. F. Dougherty, N. J. Myall, B. A. Wandell, and H. M. Feldman, "Tract Profiles of White Matter Properties: Automating Fiber-Tract Quantification," *PLoS One* 7, no. 11 (2012): 49790, https://doi.org/10.1371/journal.pone.0049790.

46. J. Gazulla, I. Benavente, A. C. Vela, et al., "New Findings in the Ataxia of Charlevoix–Saguenay," *Journal of Neurology* 259, no. 5 (2012): 869–878, https://doi.org/10.1007/s00415-011-6269-5.

47. M. Bach, F. B. Laun, A. Leemans, et al., "Methodological Considerations on Tract-Based Spatial Statistics (TBSS)," *NeuroImage* 100 (2014): 358–369, https://doi.org/10.1016/j.neuroimage.2014.06.021.

48. F. Zhang, A. Daducci, Y. He, et al., "Quantitative Mapping of the Brain's Structural Connectivity Using Diffusion MRI Tractography: A Review," *NeuroImage* 249 (2022): 118870, https://doi.org/10.1016/j.neuroimage.2021.118870.

49. C. R. Figley, M. N. Uddin, K. Wong, J. Kornelsen, J. Puig, and T. D. Figley, "Potential Pitfalls of Using Fractional Anisotropy, Axial Diffusivity, and Radial Diffusivity as Biomarkers of Cerebral White Matter Microstructure," *Frontiers in Neuroscience* 15 (2022): 799576, https://doi.org/10.3389/fnins.2021.799576.

50. C. Pierpaoli, A. Barnett, S. Pajevic, et al., "Water Diffusion Changes in Wallerian Degeneration and Their Dependence on White Matter Architecture," *NeuroImage* 13, no. 6 (2001): 1174–1185, https://doi.org/10.1006/nimg.2001.0765.

51. K. Kneer, S. Straub, J. Wittlinger, et al., "Neuropathy in ARSACS Is Demyelinating but Without Typical Nerve Enlargement in Nerve Ultrasound," *Journal of Neurology* 271, no. 5 (2024): 2494–2502, https://doi.org/10.1007/s00415-023-12159-2.

52. J.-P. Bouchard, "Recessive Spastic Ataxia of Charlevoix-Saguenay," in *Hereditary Neuropathies and Spinocerebellar Atrophies. Handbook of Clinical Neurology*, vol. 16, ed. J. M. B. V. de Jong (Elsevier, 1991), 451–459.

53. S. Cocozza, G. Pontillo, G. De Michele, et al., "Conventional MRI Findings in Hereditary Degenerative Ataxias: A Pictorial Review," *Neuroradiology* 63, no. 7 (2021): 983–999, https://doi.org/10.1007/s00234-021-02682-2.

Supporting Information

Additional supporting information can be found online in the Supporting Information section.